iScience

CellPress
OPEN ACCESS

Article

Inhibition of RIPK1 alleviating vascular smooth muscle cells osteogenic transdifferentiation via Runx2

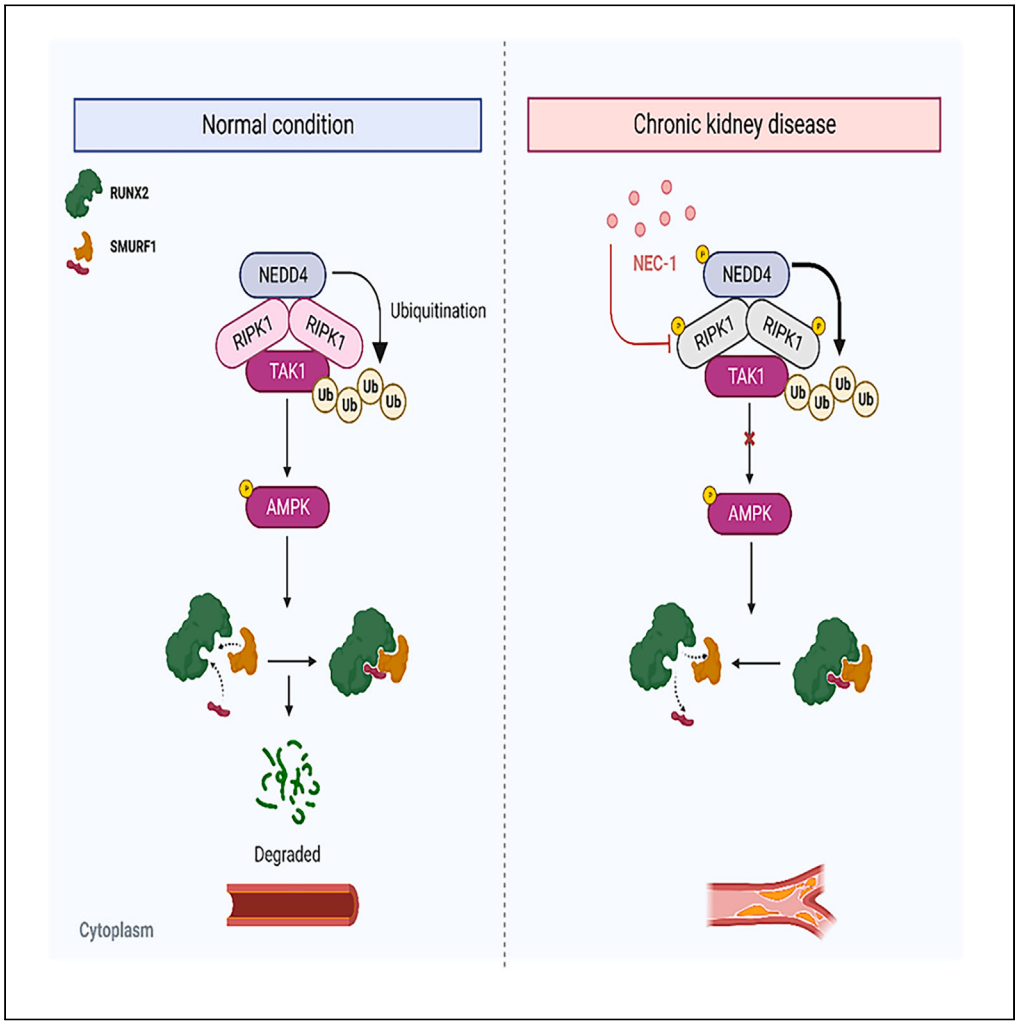

Yue Li, Wei Jie, Yanli Qi, Mingxing Mo, Yaxin Lian, Li Yin, Hui Huang

huangh8@mail.sysu.edu.cn

Highlights

RIPK1 was activated in calcified arterial tissue

Activation of RIPK1 promotes vascular calcification

NEC-1 inhibits vascular calcification via RUNX2

Phosphorylation of NEDD4 correlates with the activation of RIPK1

Li et al., iScience 27, 108766
February 16, 2024
https://doi.org/10.1016/j.isci.2023.108766

iScience

CellPress
OPEN ACCESS

Article

Inhibition of RIPK1 alleviating vascular smooth muscle cells osteogenic transdifferentiation via Runx2

Yue Li,[1,2] Wei Jie,[1,2] Yanli Qi,[1,2] Mingxing Mo,[1] Yaxin Lian,[1] Li Yin,[1] and Hui Huang[1,3,*]

SUMMARY

Vascular calcification (VC) is recognized as a crucial risk factor for cardiovascular diseases. Our previous report revealed that the osteogenic transdifferentiation of vascular smooth muscle cells (VSMCs) plays a role in this process. However, the underlying molecular mechanisms remain elusive. Notably, receptor-interacting protein kinase 1 (RIPK1) has been implicated in the development of cardiovascular diseases, yet its role and mechanisms in VC remain unexplored. To address this gap, we established models using chronic kidney disease mice and calcifying VSMCs to investigate the impact of RIPK1 on VC. Subsequently, a RIPK1-specific inhibitor (NEC-1) was applied in both *in vitro* and *in vivo* models. Our findings indicate significant activation of RIPK1 in calcified human arterial tissue, as well as in animal and cellular models. RIPK1 activation promotes the osteogenic transdifferentiation of VSMCs. Treatment with the NEC-1 substantially reduced VC. These results demonstrate that RIPK1 is a target for preventing VC.

INTRODUCTION

In recent decades, the incidence of cardiovascular diseases has increased rapidly, posing a significant threat to global public health.[1,2] Vascular calcification (VC), particularly tunica media calcification, is prevalent in chronic kidney disease (CKD) patients,[3–5] and its severity increases with the progression of the disease.[6,7] Once considered passive and degenerative, VC is now recognized as an active process that resembles the differentiation of mesenchymal cells into osteoblasts during bone formation.[8] It is widely accepted that the differentiation of vascular smooth muscle cells (VSMCs) from a contractile to an osteogenic phenotype is a major factor in the development of VC.[9]

Moreover, the stability of RUNX2 plays a role in osteogenic transdifferentiation of VSMCs.[10] RUNX2 is a crucial transcription factor that plays a pivotal role in various biological processes, particularly in skeletal development and maintenance. However, the functions of RUNX2 extend beyond its epigenetic regulatory role and also involve the regulation of its stability. The stability of RUNX2 is of paramount importance for its biological functions. Normal cellular signaling typically includes the regulation of RUNX2 stability to ensure its proper role in cell fate and differentiation. Therefore, understanding and studying the stability of RUNX2 are essential for a deeper comprehension of cellular signaling pathways and the pathogenic mechanisms of related diseases. In this study, we will focus on exploring the factors and mechanisms associated with the stability of RUNX2 to unveil its critical role in cellular regulation. In addition, vascular lesions with ruptured calcified vessels are identified as a leading cause of acute coronary syndrome events in current clinical conditions.[11] Despite its clinical significance, there are no effective interventions for arterial calcification due to a lack of comprehensive understanding of its pathogenesis.

Receptor-interacting protein kinase 1 (RIPK1) is a key regulator of cell fate determination. RIPK1 has both kinase and scaffold functions[12,13] that are independent of each other. RIPK1 is critical in regulating apoptosis and necroptosis, as well as the inflammation.[14] RIPK1 kinase promotes the development of apoptosis or necroptosis, depending on the cellular context and molecules with which it interacts. Unlike its kinase function, which promotes cell death, its scaffold function promotes cell survival by mediating the activation of nuclear factor kappa-light-chain-enhancer of activated B cells (NF-κB) and mitogen-activated protein kinase(MAPK) signaling pathways.[15,16] Necrostatin-1 (NEC-1) is a small-molecule inhibitor of RIPK1 kinase and has been widely used to study the role of RIPK1 in mechanistic studies of human diseases and animal models. The general therapeutic use of RIPK1 inhibitors in treating a variety of human diseases, such as psoriasis, rheumatoid arthritis, ulcerative colitis, and amyotrophic lateral sclerosis, is being investigated in clinical trials.[17,18]

This study aimed to investigate the role and underlying molecular mechanism of RIPK1 in VC. Clinical samples from CKD patients were used to examine the role of RIPK1 phosphorylation in calcified arteries. We explored the effect of RIPK1 on VC both *in vivo* and *in vitro* experiments, and the underlying molecular mechanism was detailed. The results showed that RIPK1 activation promoted VC, and the small-molecule inhibitor

[1]Cardiovascular Department, The Eighth Affiliated Hospital, Joint Laboratory of Guangdong-Hong Kong-Macao Universities for Nutritional Metabolism and Precise Prevention and Control of Major Chronic Diseases, Sun Yat-sen University, Shenzhen, China
[2]These authors contributed equally
[3]Lead contact
*Correspondence: huangh8@mail.sysu.edu.cn
https://doi.org/10.1016/j.isci.2023.108766

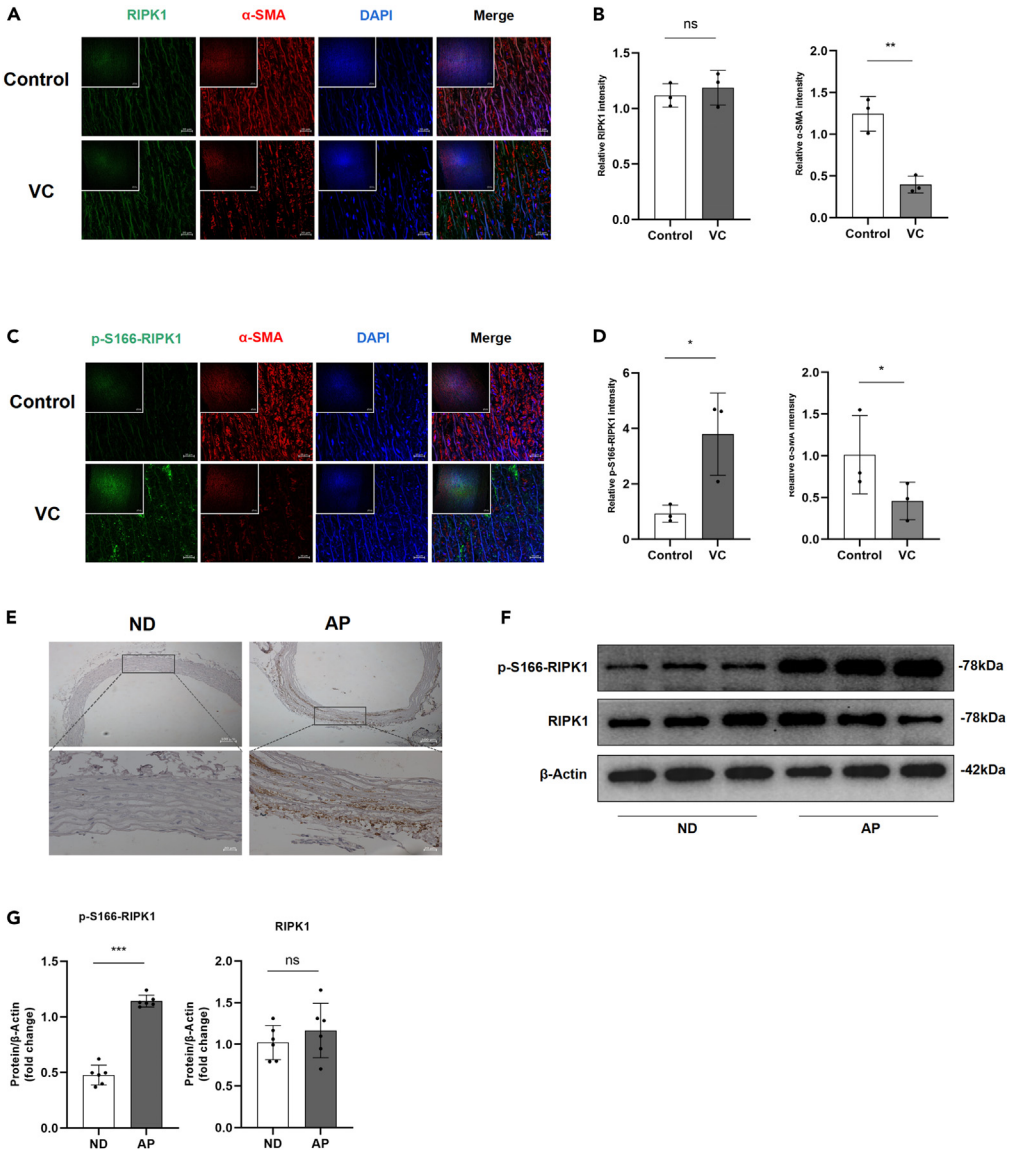

Figure 1. RIPK1 was activated in calcified arterial tissue

(A and B) Expression levels and quantification analysis of RIPK1 in human arteries of indicated groups were determined by IF staining (n = 3 per group). Bar = 20 um.

(C and D) Expression levels and quantification analysis of p-S166-RIPK1 in human arteries of indicated groups were determined by IF staining (n = 3 per group). Bar = 20 um.

(E) Expression cation analysis of p-S166-RIPK1 in mice abdominal aortic arteries of indicated groups were determined by IHC staining (n = 5 per group). Bar = 20 um.

(F and G) Western blot analysis and quantification of p-S166-RIPK1 and RIPK1 expression in mice abdominal aortic arteries (n = 6 per group). Results are presented as mean ± SEM, and analyzed using two-way ANOVA with Tukey's *post hoc* test. *p < 0.05, **p < 0.01, ***p < 0.001, ****p < 0.0001; ns indicates p > 0.05.

NEC-1 significantly reduced VC in both *in vitro* and *in vivo* models. These findings highlight the critical role of RIPK1 in the osteogenic transdifferentiation of VSMCs, and it may serve as a potential therapeutic target for VC induced by CKD.

RESULTS

RIPK1 was activated in calcified arterial tissue

Immunofluorescence (IF) results showed that there was no significant change in total RIPK1 expression in calcified human blood vessels and normal human blood vessels (Figures 1A and 1B), but the expression of p-S166-RIPK1, a marker of RIPK1 activation, was significantly increased

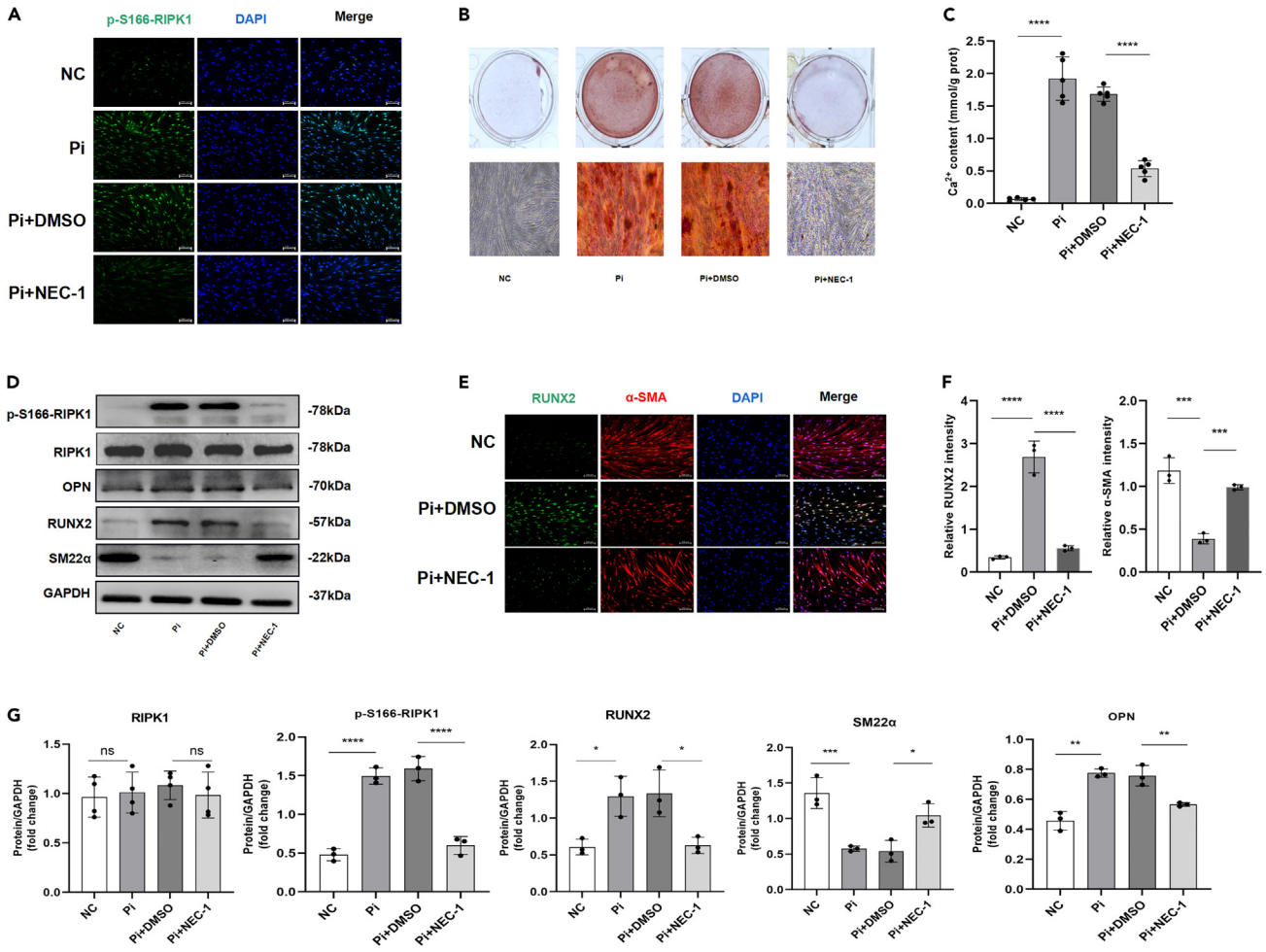

Figure 2. RIPK1 activation promotes osteogenic transdifferentiation of VSMCs

(A) VSMCs were added with DMSO or NEC-1 and then incubated with Pi (3.0 mM) for 7 days; IF staining was performed for p-S166-RIPK1. Bar = 100 um.

(B) VSMCs were exposed to Pi (3.0 mM) for 7 days and then stained for mineralization by alizarin red S.

(C) VSMCs were exposed to Pi (3.0 mM) for 7 days and then quantitative analysis of calcium content.

(D and G) VSMCs were added with DMSO or NEC-1 and then incubated with Pi (3.0 mM) for 7 days, and the downstream osteogenic markers (OPN, RUNX2) and contractile property markers (SM22) were analyzed by western blot (n = 3 per group). p-S166-RIPK1 and RIPK1 protein expression was also detected.

(E and F) VSMCs were added with DMSO or NEC-1 and then incubated with Pi (3.0 mM) for 7 days; IF staining was performed for RUNX2 and α-SMA. Bar = 100 um.

Results are presented as mean ± SEM and analyzed using two-way ANOVA with Tukey's Alizarin test. *p < 0.05, **p < 0.01, ***p < 0.001, ****p < 0.0001; ns indicates p > 0.05.

(Figures 1C and 1D). The basic information of clinical samples is shown in Table S1. The results showed that RIPK1 was activated in calcified human blood vessels. To gain further insight into the role of RIPK1 in VC, we induced VC in wild-type (WT) mice through 2 CKD models (high adenine and phosphorus [AP] model and vitamin D [VD] model). The basic conditions of WT and CKD mice are shown in Figures S1 and S2. And immunohistochemical (IHC) staining results showed that p-S166-RIPK1 expression was significantly increased in calcified media vascular tissues of AP-diet mice compared with normal-diet (ND) mice (Figure 1E). Moreover, western blot (WB) results also showed that the expression of p-S166-RIPK1 was significantly increased in calcified vessels, but the total RIPK1 expression level was unchanged (Figures 1F and 1G). These data indicate that RIPK1 is activated in VC.

RIPK1 promotes high phosphate-induced osteogenic transdifferentiation of VSMCs

We performed further experiments to investigate the role of RIPK1 on VC *in vitro*. IF results showed that NEC-1 could significantly reduce the expression of p-S166-RIPK1, indicating that NEC-1 inhibition was effective (Figure 2A). *In vitro*, we observed that treatment with Pi (3.0 mmol/L) led to increased calcium deposition in VSMCs, but the addition of NEC-1 resulted in lower calcium deposition as confirmed by alizarin red staining and calcium content determination (Figures 2B and 2C). Western blot analysis showed that the expression of

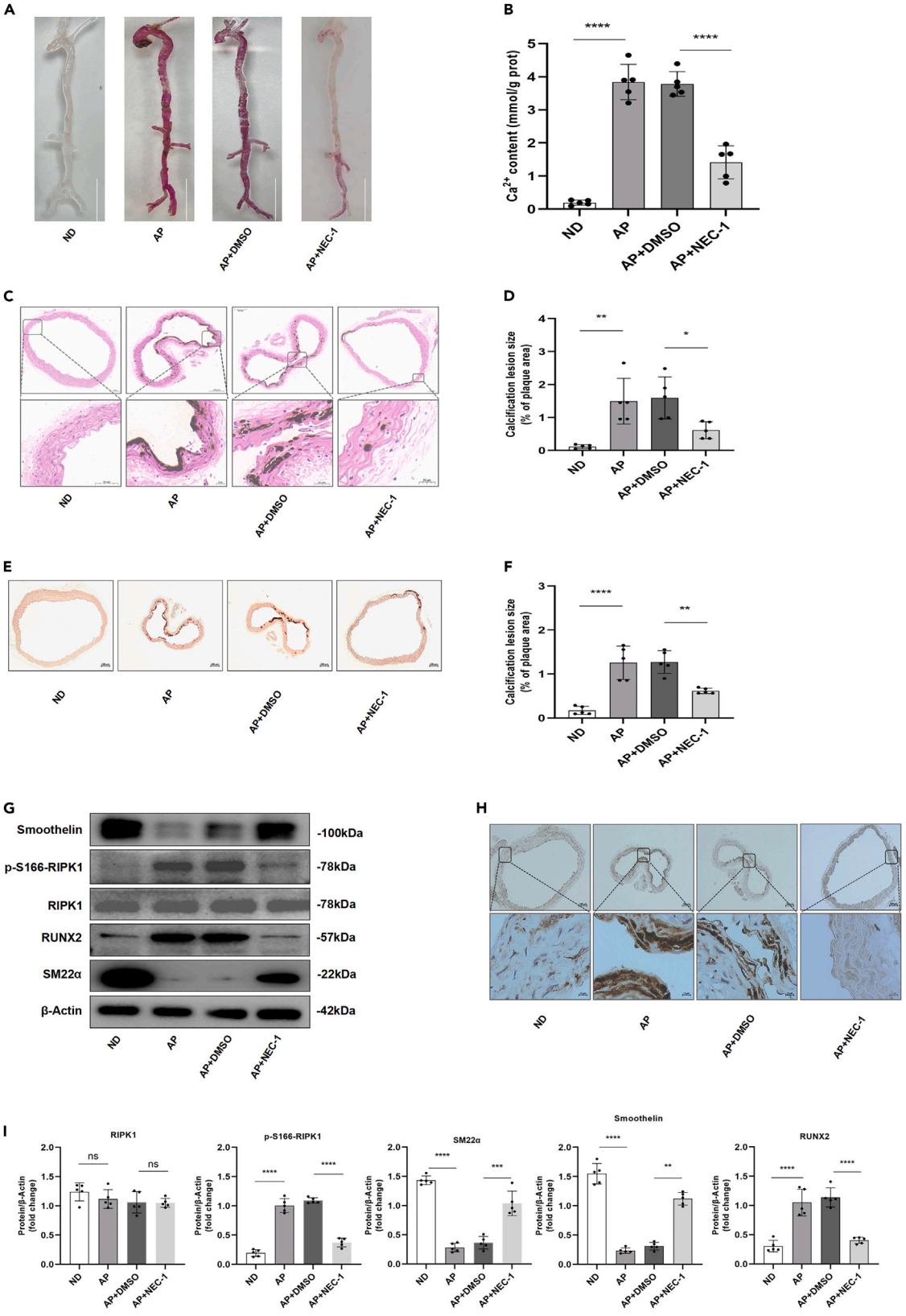
A
ND
AP
AP+DMSO
AP+NEC-1
B
Ca2+ content (mmol/g prot)
****
****
C
D
Calcification lesion size (% of plaque area)
**
*
E
F
Calcification lesion size (% of plaque area)
****
**
G
Smoothelin
p-S166-RIPK1
RIPK1
RUNX2
SM22α
β-Actin
-100kDa
-78kDa
-78kDa
-57kDa
-22kDa
-42kDa
H
I
RIPK1
p-S166-RIPK1
SM22α
Smoothelin
RUNX2
Protein/β-Actin (fold change)
ns
ns

Figure 3. RIPK1 activation promotes vascular calcification *in vivo*

(A) WT mice were intraperitoneally injected with NEC-1(1.8 mg/kg). Then these mice were treated with an adenine and phosphorus (AP) diet for 12 weeks. Then the mice were sacrificed and aortas were collected. Alizarin red S images showing calcification in the aortas among these groups. The calcified parts of the aorta were shown in deep purple. Scale bars: 100 μm (B) Calcium content were quantified in aortas tissue among these groups.

(C and D) Representative von Kossa staining of abdominal aorta sections (n = 4 per group). Scale bars: 100 μm.

(E and F) Representative alizarin red S of abdominal aorta sections (n = 4 per group). Scale bars: 100 μm (G and I) Analysis of osteogenic and contractile property factor expression of aortas tissue among these groups by western blot. p-S166-RIPK1 and RIPK1 protein expression was also detected.

(H) Expression levels of RUNX2 in abdominal arteries of indicated groups were determined by IHC staining (n = 4 per group). Bar = 100 μm. Results are presented as mean ± SEM and analyzed using two-way ANOVA with Tukey's *post hoc* test. *p < 0.05, **p < 0.01, ***p < 0.001, ****p < 0.0001; ns indicates p > 0.05.

p-S166-RIPK1 was significantly increased in VSMCs treated with high phosphorus, and the expression was decreased by the addition of NEC-1, but the total RIPK1 expression level was unchanged; this suggests that RIPK1 is also activated in VSMCs calcification model induced by high phosphorus. Moreover, inhibition of RIPK1 activity reduced the expression of osteogenic phenotype markers osteopontin (OPN) and RUNX2 and increased the expression of contractile phenotype marker smooth muscle contractile protein 22α (SM22α) (Figures 2D and 2F). The results of IF assay also showed that NEC-1 could downregulate RUNX2 expression in VSMCs calcification model, which was consistent with the results of western blot (Figure 2E). These results suggest that RIPK1 activation can exacerbate VC *in vitro*, while NEC-1 administration can significantly reduce calcification levels by inhibiting RIPK1 kinase phosphorylation.

RIPK1 activation promotes VC *in vivo*

To further verify the promoting effect of RIPK1 in VC, we induced VC in WT mice through 2 CKD models (high AP model and VD model), and in the treatment group by intraperitoneal injection of NEC-1 and Necrostatin-1s (NEC-1s). As determined by alizarin red staining of blood vessels and tissue calcium content, VC was significantly aggravated in CKD model, while it was significantly reduced by NEC-1 or NEC-1s intraperitoneal injection (Figures 3A, 3B, S3A, and S3B). von Kossa assays and alizarin red results of the vascular ring also showed that VC was significantly aggravated in the CKD model, while it was significantly reduced by NEC-1 intraperitoneal injection (Figures 3C–3F). As expected, inhibition of RIPK1 activation could downregulate the expression of RUNX2 and upregulate the expression of SM22α and Smoothelin (Figures 3G, 3I, S3C, and S3D). IHC results also showed that the expression of RUNX2 increased in the CKD model group but decreased significantly in the NEC-1 treatment group (Figure 3H). Taken together, these results indicate that RIPK1 activation plays a crucial role in promoting VC *in vivo*, which can be partially reversed by the inhibition of RIPK1 activation.

RIPK1 promotes RUNX2 degradation through the ubiquitination-proteasome pathway

Osteogenic transdifferentiation of VSMCs plays a crucial role in the formation of VC. In this study, we aimed to explore the mechanism of RIPK1 in this process. Since the osteogenic transdifferentiation of VSMCs was highly regulated by RUNX2,[19,20] we investigated whether RIPK1 regulates VC through RUNX2. The expression of RUNX2 was significantly downregulated with the decrease of p-S166-RIPK1 expression *in vitro* and *in vivo* (Figures 2D, 3E, S4A, and S4B). Additionally, overexpression of RUNX2 removed the protective capacity of NEC-1(Figures 4A and 4B). These results demonstrated that the RIPK1 is a crucial factor that promotes the process of osteogenic transdifferentiation in VSMCs by upregulating the expression of RUNX2.

In order to identify the mechanism by which RIPK1 regulates RUNX2, quantitative PCR (qPCR) was used to determine whether the transcription level of RUNX2 was affected by RIPK1. The results showed no significant difference in the mRNA level of RUNX2 between the high-phosphorus group and the NEC-1 treatment group, indicating that RIPK1 activation had no effect on the transcription level of RUNX2 (Figure 4C). Previous studies have shown that there are many types of post-translational modifications of RUNX2 that determine its stability. In addition, ubiquitination plays a role in this process.[6,10] To determine whether RIPK1 activation affects the ubiquitination of RUNX2, we treated VSMCs with the protein synthesis inhibitor cycloheximide (CHX) and observed the stability of RUNX2. The results showed that the stability of RUNX2 was decreased in the NEC-1 group (Figures 4D and 4E). Proteasome inhibitor MG132 and autophagy inhibitor 3-MA were used to explore the degradation mode of RUNX2. MG132 blocked RUNX2 degradation (Figures 4F and 4G), but 3-MA did not (Figures 4I and 4J), which proved that the degradation of RUNX2 was mediated by the proteasome rather than the lysosome. Proteasomal degradation of proteins is often associated with the specific ubiquitylation of target proteins. Consequently, we investigated the level of ubiquitination of RUNX2 in different groups and found that the ubiquitination level of RUNX2 was downregulated in VSMCs with high-phosphorus conditions and upregulated after NEC-1 treatment (Figure 4H), indicating that RIPK1 may affect the stability of RUNX2 via ubiquitination. Furthermore, we explored the expression of SMURF1, an E3 ubiquitin ligase that is involved in the ubiquitination degradation of RUNX2, as well as its interaction with RUNX2.[21] We found little difference in SMURF1 expression between the control group and the NEC-1 group (Figures 4L and 4M). However, the interaction between SMURF1 and RUNX2 was weaker in the high-phosphorus group compared to the NEC-1 group (Figure 4K). Taken together, these data suggest that RIPK1 activation affects the stability of RUNX2 via its regulation of the ubiquitination.

RIPK1 activation mediates the ubiquitination and degradation of RUNX2 through TAK1-AMPK pathway

To gain further insights into the mechanism by which RIPK1 activation inhibits the ubiquitination and degradation of RUNX2, we investigated whether it operates via the AMPK pathway, as activated AMPK has been shown to promote the binding of SMURF1 to RUNX2,

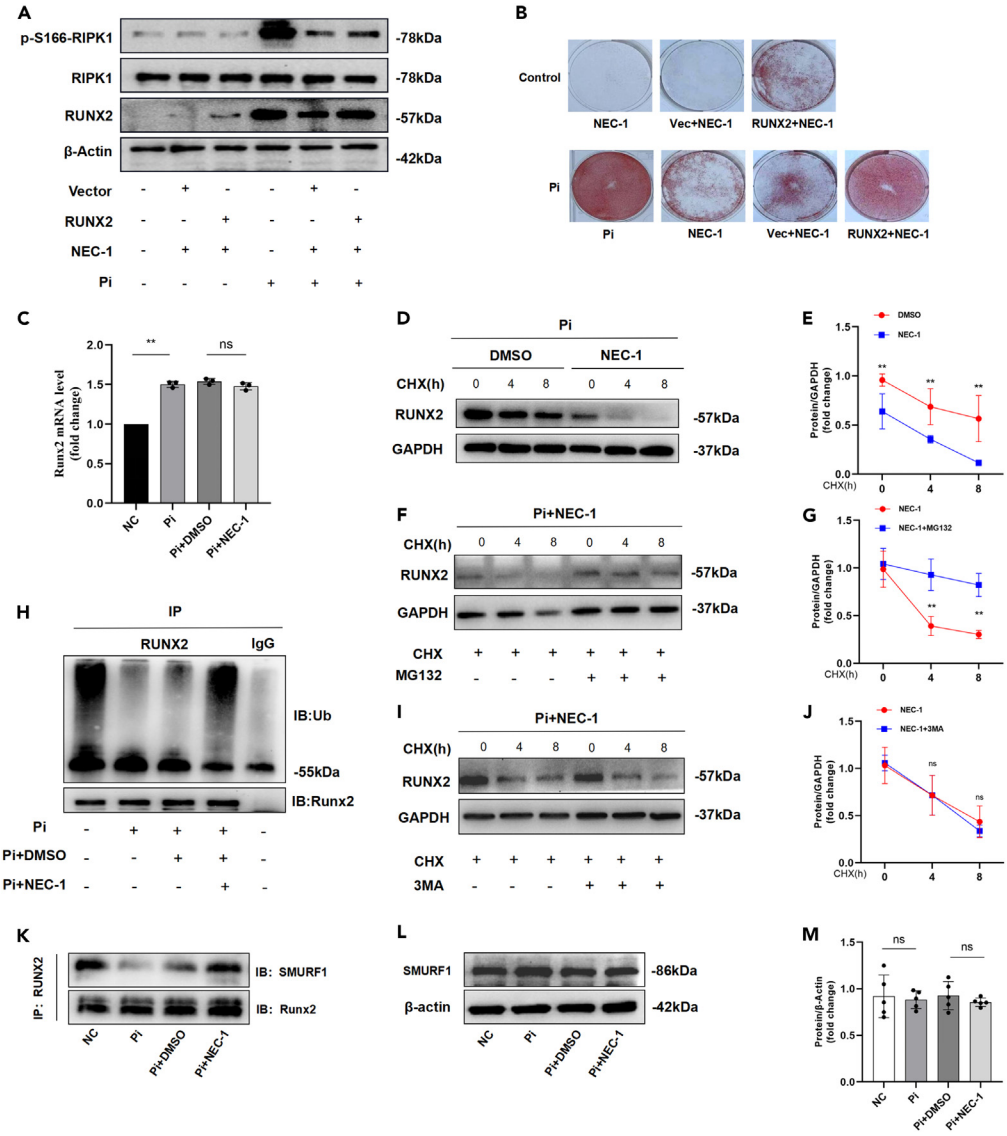

Figure 4. RIPK1 activation inhibits RUNX2 degradation through the ubiquitination-proteasome pathway

(A) VSMCs were pretransfected with RUNX2 plasmid or vector plasmid and then exposed to Pi (3.0 mM) for 7 days. The expression of RIPK1 and RUNX2 was analyzed by western blot.

(B) VSMCs were stained for mineralization by alizarin red S.

(C) Quantitative reverse-transcription polymerase chain reaction (RT-qPCR) analysis of RUNX2 mRNA expression in human VSMCs in indicated groups.

(D and E) RIPK1 kinase activity was inhibited in VSMCs by NEC-1 together with Pi (3.0 mM) incubation for 7 days. VSMCs were treated with Pi (3.0 mM) for 7 days and incubated with the protein translation inhibitor CHX (0.2 mM) for the indicated times before harvest, followed by immunoblotting with the anti-RUNX2 antibody and anti-GAPDH antibody. The curve shows the stability of the protein of RUNX2.

(F and G) VSMCs added NEC-1(10 μM) were incubated with Pi (3.0 mM) together with the MG132 (10 μM) or 3-MA (1.5 μM) for 7 days (I and J), and then the protein translation inhibitor CHX (0.2 mM) was added for the indicated times before harvest, followed by immunoblotting with the anti-RUNX2 antibody and anti-GAPDH antibody. The curve shows the stability of RUNX2 protein.

(H) VSMCs in different groups were immunoprecipitated with anti-RUNX2 antibody and immunoblotted with anti-ubiquitin (anti-Ub) antibody.

(K) Anti-RUNX2 IP followed by WB with anti-RUNX2 and anti-SMURF1 antibody in VSMCs in different groups after treatment with Pi for 7days. (L and M) Analysis of E3 ubiquitin ligase SMURF1 among these groups by western blot. Results are presented as mean ± SEM and analyzed using two-way ANOVA with Tukey's *post hoc* test. *p < 0.05, **p < 0.01, ***p < 0.001, ****p < 0.0001; ns indicates p > 0.05.

leading to its ubiquitination and degradation.[22,23] Our results showed that RIPK1 activation decreased the phosphorylation of AMPK, which indicates its activation (Figures 5A and 5B). Moreover, transfection with siAMPK partially reversed the inhibitory effect of NEC-1 on calcification and upregulated the expression level of RUNX2 protein (Figures 5C and 5D). Consistent with these results, alizarin red staining

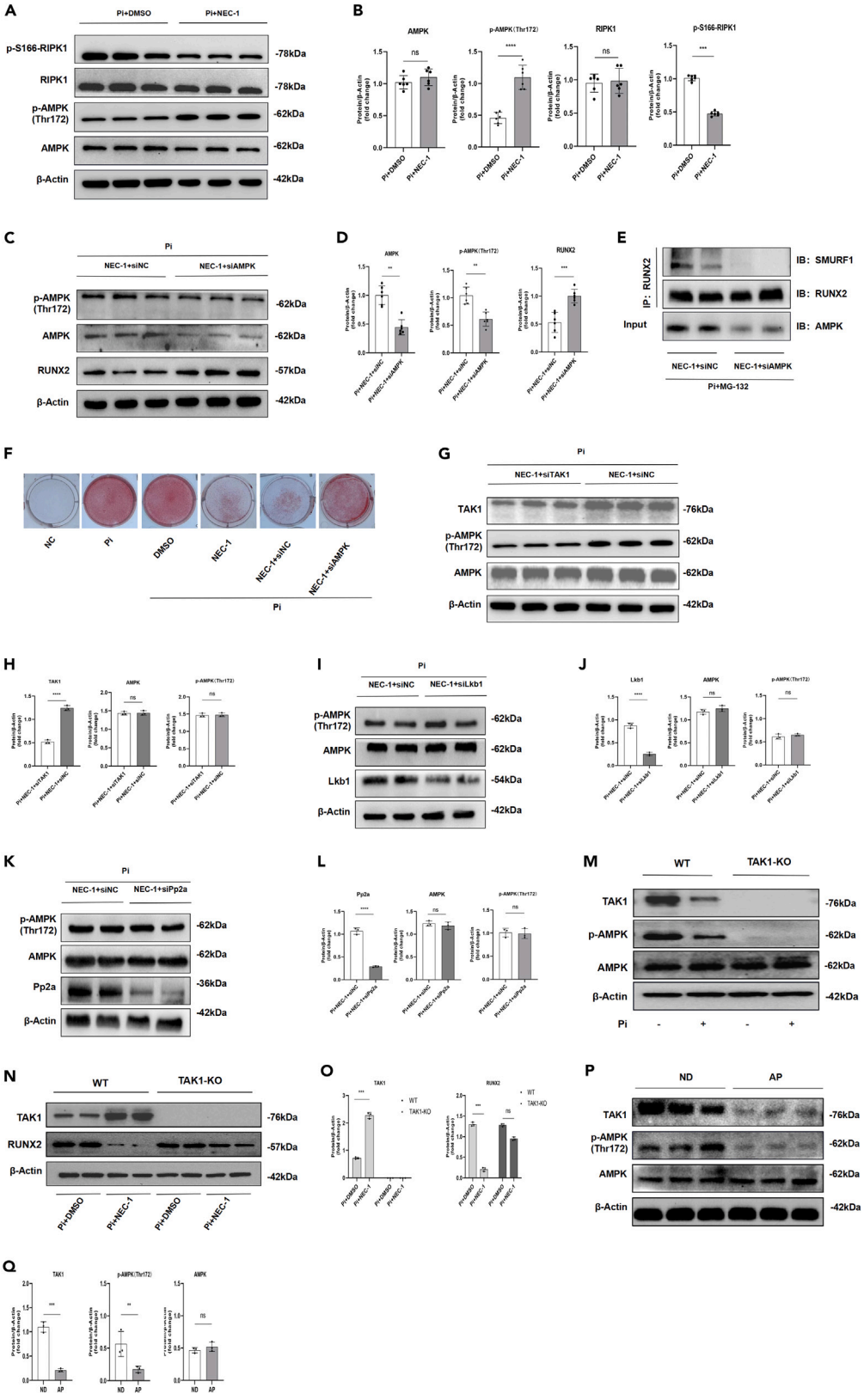
A
Pi+DMSO
Pi+NEC-1
p-S166-RIPK1
RIPK1
p-AMPK (Thr172)
AMPK
β-Actin
-78kDa
-78kDa
-62kDa
-62kDa
-42kDa
B
AMPK
p-AMPK(Thr172)
RIPK1
p-S166-RIPK1
ns
****
ns
***
Protein/β-Actin (fold change)
Pi+DMSO
Pi+NEC-1
C
Pi
NEC-1+siNC
NEC-1+siAMPK
p-AMPK (Thr172)
AMPK
RUNX2
β-Actin
-62kDa
-62kDa
-57kDa
-42kDa
D
AMPK
p-AMPK(Thr172)
RUNX2
**
**
***
E
IP: RUNX2
Input
IB: SMURF1
IB: RUNX2
IB: AMPK
NEC-1+siNC
NEC-1+siAMPK
Pi+MG-132
F
NC
Pi
DMSO
NEC-1
NEC-1+siNC
NEC-1+siAMPK
Pi
G
Pi
NEC-1+siTAK1
NEC-1+siNC
TAK1
p-AMPK (Thr172)
AMPK
β-Actin
-76kDa
-62kDa
-62kDa
-42kDa
H
TAK1
AMPK
p-AMPK(Thr172)
****
ns
ns
I
Pi
NEC-1+siNC
NEC-1+siLkb1
p-AMPK (Thr172)
AMPK
Lkb1
β-Actin
-62kDa
-62kDa
-54kDa
-42kDa
J
Lkb1
AMPK
p-AMPK(Thr172)
****
ns
ns
K
Pi
NEC-1+siNC
NEC-1+siPp2a
p-AMPK (Thr172)
AMPK
Pp2a
β-Actin
-62kDa
-62kDa
-36kDa
-42kDa
L
Pp2a
AMPK
p-AMPK(Thr172)
****
ns
ns
M
WT
TAK1-KO
TAK1
p-AMPK
AMPK
β-Actin
Pi
-76kDa
-62kDa
-62kDa
-42kDa
N
WT
TAK1-KO
TAK1
RUNX2
β-Actin
-76kDa
-57kDa
-42kDa
Pi+DMSO
Pi+NEC-1
Pi+DMSO
Pi+NEC-1
O
TAK1
RUNX2
WT
TAK1-KO
***
***
ns
P
ND
AP
TAK1
p-AMPK (Thr172)
AMPK
β-Actin
-76kDa
-62kDa
-62kDa
-42kDa
Q
TAK1
p-AMPK(Thr172)
AMPK
***
**
ns
ND
AP

Figure 5. RIPK1 mediate the ubiquitination and degradation of RUNX2 through TAK1-AMPK pathway

(A and B) VSMCs added NEC-1(10 μM) were incubated with Pi (3.0 mM) for 7 days, and the downstream markers (AMPK, *p*-AMPK(Thr172)) and (RIPK1, p-S166-RIPK1) were analyzed by western blot (n = 6 per group).

(C and D) VSMCs added NEC-1(10 uM) were transfected with siAMPK or siNC and then incubated with Pi (3.0 mM) for 7 days, and the RUNX2 protein expression were analyzed by western blot (n = 6 per group).

(E) VSMCs in different groups were immunoprecipitated with anti-RUNX2 antibody and immunoblotted with anti-SMURF1 antibody(n = 3 per group).

(F) VSMCs were stained for mineralization by alizarin red S (n = 3 per group).

(G–L) VSMCs added NEC-1(10 uM) were transfected with siTAK1, LKB1, and siPp2a and then incubated with Pi (3.0 mM) for 7 days, and the AMPK and *p*-AMPK(Thr172) protein expression was analyzed by western blot (n = 3 per group).

(M) TAK1 and *p*-AMPK(Thr172) expression was analyzed in WT and TAK1-KO VSMCs after Pi (3.0 mM) treatment by western blot (n = 3 per group).

(N and O) TAK1 and RUNX2 expression was analyzed in WT and TAK1-KO VSMCs after NEC-1 treatment by western blot (n = 3 per group).

(P and Q) Western blot analysis and quantification of TAK1 and *p*-AMPK(Thr172) and AMPK expression in mice abdominal aortic arteries (n = 3 per group). Results are presented as mean ± SEM and analyzed using two-way ANOVA with Tukey's *post hoc* test. *p < 0.05, **p < 0.01, ***p < 0.001, ****p < 0.0001; ns indicates p > 0.05.

showed a similar trend (Figure 5F). In addition, we found that in the NEC-1 treatment group, knocking down AMPK significantly reduced SMURF1 and RUNX2 binding (Figure 5E). These results suggest that inhibition of RIPK1 activation reduces RUNX2 protein expression through the AMPK pathway.

TAK1, Lkb1, and Pp2a are known to be the major upstream kinases responsible for AMPK phosphorylation and subsequent activation.[24,25] To identify the major upstream kinases that mediate the downregulation of AMPK activity in the presence of RIPK1 activation, we performed gene knockdown experiments. The results showed that the phosphorylation level and activity of AMPK decreased only when TAK1 was knocked down (Figures 5G and 5H), while Lkb1 and Pp2a had no significant effect on AMPK activity (Figures 5I–5L). To further verify that TAK1 is the main upstream kinase that activates AMPK, we successfully constructed the TAK1-knockout VSMCs line. The results showed that AMPK activity was significantly inhibited in TAK1-knockout cells (Figure 5M), and the downregulation of RUNX2 protein expression by NEC-1 was reversed (Figures 5N and 5O). The results were consistent in *in vitro* and *in vivo* models. Compared with ND group, the expression of TAK1 was significantly downregulated and the activation of AMPK was inhibited in the vascular tissues of the AP-diet mice (Figures 5P and 5Q). The results were consistent in *in vitro* and *in vivo* models. Taken together, these data indicated that TAK1 was the key upstream kinase of RIPK1 affecting AMPK activity. Collectively, these findings suggest that RIPK1 activation increases the expression of RUNX2 through the TAK1-AMPK pathway.

Phosphorylation of NEDD4 correlates with the activation of RIPK1

Previous studies have shown that RIPK1 interacts with TAK1.[13] However, the effect of RIPK1 activity on TAK1 expression level needs to be confirmed by further experiments. Inhibition of RIPK1 activation reversed the downregulation of TAK1 expression (Figures 6A and 6B). In addition, silencing of TAK1 reversed the downregulation of RUNX2 that was induced by the inhibition of RIPK1 activation (Figures 6C and 6D). Further immunoprecipitation (IP) experiments demonstrated that TAK1 knockdown led to the restoration of RUNX2 ubiquitination, which had been induced by NEC-1 (Figure 6E). This implies that the downregulation of TAK1 expression is partly due to RIPK1 activation. Furthermore, TAK1 is required for RIPK1 activation to induce the alteration of RUNX2 expression.

The regulatory mechanism of RIPK1 activation on TAK1 was further investigated. We performed experiments to measure TAK1 ubiquitination levels. The mRNA levels of TAK1 were not significantly different among the four groups (Figure 6F). And the level of TAK1 ubiquitination increased under high-phosphorus conditions, while the level of TAK1 ubiquitination decreased after treatment with NEC-1 (Figure 6G). This suggests that the activity of RIPK1 affects the ubiquitination level of TAK1 in VSMCs.

We next investigated which E3 ubiquitin ligase mediated the protein degradation of TAK1 induced by RIPK1 activation. Previous studies have shown that NEDD4 is an E3 ubiquitin ligase that regulates TAK1 ubiquitination and degradation.[21] Consistently, NEDD4 is predicted as a primary E3 ligase for TAK1 in the UbiBrowser database (Figure S5). This was also confirmed by our results (Figures 6H and 6I). IP assay confirmed the existence of RIPK1/NEDD4/TAK1 complex (Figure 6J). Moreover, immunocoprecipitation results showed that inhibition of RIPK1 activation by NEC-1 could reduce the ubiquitination degree of TAK1, and the ubiquitination degree of TAK1 was further reduced after NEDD4 knockdown (Figure 6K). In addition, we found that overexpression of NEDD4 decreased TAK1 protein expression and AMPK activity, while, with the increase of overexpression of NEDD4, the downregulation effect of NEC-1 on RUNX2 was gradually weakened (Figures 6L and 6M). It has been reported that NEDD4 can be phosphorylated to greatly improve its ubiquitination capacity.[26] Both NEDD4 and RIPK1 were phosphorylated at high levels in VSMCs under high-phosphorus stimulation, which were substantially reduced when RIPK1 activation was inhibited (Figure 6N). We observed a significant correlation between the phosphorylation levels of NEDD4 and the kinase activity of RIPK1. However, further research is needed to determine the specific mechanisms underlying their interaction.

DISCUSSION

The main finding of this study is the significant contribution of RIPK1 in VC, which was demonstrated for the time. The study uncovered a RIPK1/RUNX2 pathway in VC, where RIPK1 activation was shown to promote VSMCs osteogenic transdifferentiation from a contractile to an osteogenic phenotype. Mechanistically, the study showed that RIPK1 activation enhanced the ubiquitination degradation of TAK1 by

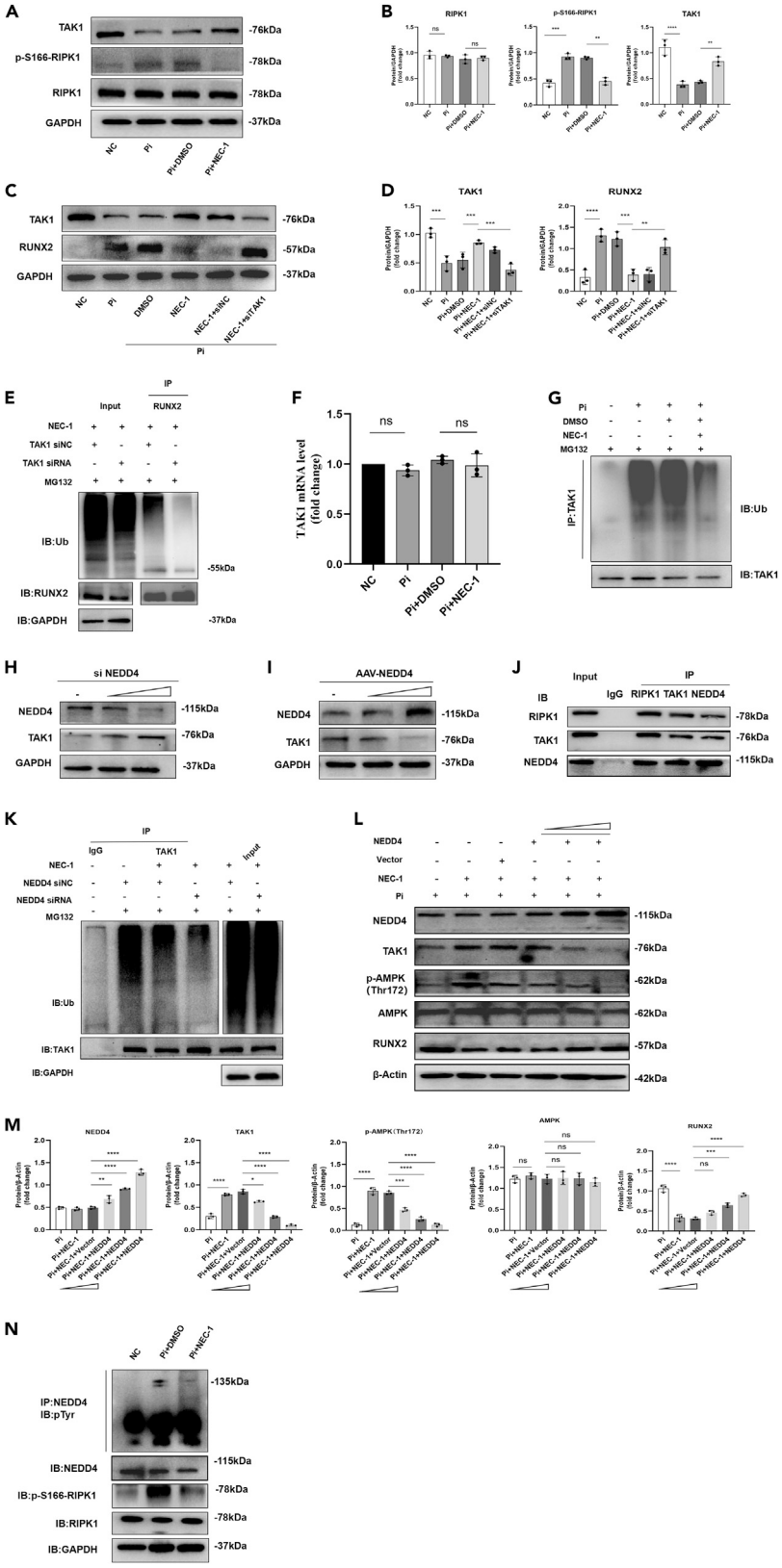
A
TAK1
p-S166-RIPK1
RIPK1
GAPDH
-76kDa
-78kDa
-78kDa
-37kDa
NC
Pi
Pi+DMSO
Pi+NEC-1
B
RIPK1
p-S166-RIPK1
TAK1
ns
C
TAK1
RUNX2
GAPDH
-76kDa
-57kDa
-37kDa
NC
Pi
DMSO
NEC-1
NEC-1+siNC
NEC-1+siTAK1
Pi
D
TAK1
RUNX2
Pi+NEC-1+siNC
Pi+NEC-1+siTAK1
E
IP
Input
RUNX2
NEC-1
TAK1 siNC
TAK1 siRNA
MG132
IB:Ub
IB:RUNX2
IB:GAPDH
-55kDa
-37kDa
F
TAK1 mRNA level (fold change)
ns
G
Pi
DMSO
NEC-1
MG132
IP:TAK1
IB:Ub
IB:TAK1
H
si NEDD4
NEDD4
TAK1
GAPDH
-115kDa
-76kDa
-37kDa
I
AAV-NEDD4
J
Input
IP
IB
IgG
RIPK1
TAK1
NEDD4
K
IP
IgG
TAK1
Input
NEC-1
NEDD4 siNC
NEDD4 siRNA
MG132
IB:Ub
IB:TAK1
IB:GAPDH
L
NEDD4
Vector
NEC-1
Pi
TAK1
p-AMPK (Thr172)
AMPK
RUNX2
β-Actin
-62kDa
-57kDa
-42kDa
M
NEDD4
TAK1
p-AMPK(Thr172)
AMPK
RUNX2
Protein/β-Actin (fold change)
N
IP:NEDD4
IB:pTyr
IB:NEDD4
IB:p-S166-RIPK1
IB:RIPK1
IB:GAPDH
-135kDa

Figure 6. Phosphorylation of NEDD4 correlates with the activation of RIPK1

(A and B) Analysis of TAK1 protein expression among these groups by western blot. p-S166-RIPK1 and RIPK1 protein expression was also detected (n = 3 per group).

(C and D) WT and NEC-1(10 μM)-added VSMCs were incubated with Pi (3.0 mM) together with siTAK1 or siNC for 7 days, and the RUNX2 protein expression was analyzed by western blot (n = 3 per group).

(E) Human VSMCs with Scr siRNA or TAK1 siRNA transfection, NEC-1(10 uM) supplementation, were pretreated with MG132 (10 μM). The expression of RUNX2, Ub (ubiquitin), and GAPDH was determined by western blot analysis (Input). Immunoprecipitation was performed with RUNX2 antibody; RUNX2 and RUNX2-bound Ub was determined by western blot analysis (n = 3 per group).

(F) Quantitative reverse-transcription polymerase chain reaction (RT-qPCR) analysis of TAK1 mRNA expression in human VSMCs in indicated groups.

(G) VSMCs in different groups were immunoprecipitated with anti-TAK1 antibody and immunoblotted with anti-ubiquitin (anti-Ub) antibody.

(H and I) Protein expression of TAK1 in VSMCs with a dose-dependent siNEDD4 and AAV-NEDD4.

(J) Precipitation and western blot analyses showing the binding of NEDD4 to TAK1 and RIPK1 using indicated antibodies in VSMCs.

(K) VSMCs in different groups were immunoprecipitated with anti-TAK1 antibody and immunoblotted with anti-ubiquitin (anti-Ub) antibody.

(L and M) Protein expression of TAK1, p-AMPK(Thr172), AMPK, and RUNX2 in VSMCs with a dose-dependent AAV-NEDD4. (N) VSMCs in different groups were immunoprecipitated with anti-NEDD4 antibody and immunoblotted with anti-*p*-NEDD4 antibody. Results are presented as mean ± SEM and analyzed using two-way ANOVA with Tukey's post hoc test. *p < 0.05, **p < 0.01, ***p < 0.001, ****p < 0.0001; ns indicates p > 0.05.

NEDD4. Reduction of TAK1 weakens phosphorylated activation of AMPK, which in turn reduces the binding of E3 ubiquitinating enzyme SMURF1 to RUNX2, leading to reduced degradation of RUNX2 and promoting the occurrence of VC. Treatment with the RIPK1 inhibitor NEC-1 or NEC-1s can partially reverse this pathological process.

RIPK1 is mainly located in the cytoplasm and is a factor in the regulation of cell death signal. RIPK1 plays a role in a variety of biological processes and has been implicated in a range of inflammatory and aging-related diseases. Studies have shown that RIPK1 plays a catalytic role in atherosclerotic formation and inflammatory diseases.[27,28] CKD is one of the typical age-related inflammatory diseases; however, the relationship between RIPK1 and VC is unclear. Using two typical CKD model, we reported that the level of VC was significantly lower in the NEC-1- and NEC-1s-treated group than in the CKD group. RIPK1 activation can promote VC induced by Pi *in vitro*. In our clinical study, the activated form of RIPK1 (p-S166-RIPK1) was expressed at elevated levels in the calcified artery of patients. There were no significant differences in kidney function or traditional risk factors between patients with or without VC. RIPK1 plays a role in apoptosis and inflammation and may play a certain role in VC. However, we did not detect significant cell death during modeling process (Figure S4C), which may be related to osteogenic reprogramming of VSMCs.

During arterial calcification, VSMCs are highly plastic under high-phosphorus or other calcification environments, and it can differentiate into other phenotypes. These phenotypes are similar to foam cells, osteoblasts, and macrophages. A pedigree tracing study found that 98% of osteoblasts in VC lesions were derived from VSMCs.[29] Our results show that RIPK1 activation increases the expression of osteoblast protein while decreasing the expression of contractile protein *in vivo* and *in vitro*. Taken together, these features support the hypothesis that RIPK1 is involved in VSMCs osteoblastic phenotypic transition. There is strong evidence that the osteogenic differentiation of VSMCs is mainly regulated by the transcription factor RUNX2. We found that the degree of RIPK1 activity was significantly correlated with the abundance of RUNX2 in cells. Taken together, these findings strongly suggest that RIPK1 has an integral role as a "gatekeeper" to the fate of VSMCs during lineage reprogramming to osteochondrogenesis.

Upregulation of RUNX2 expression has been observed in VC, and its core role in VSMCs osteochondrogenic reprogramming has been well documented.[30,31] In the cardiovascular system, the upregulation of RUNX2 has become a regulator of cardiovascular adverse events. At present, there has been initial progress in the treatment of RUNX2 intervention to delay VC at the animal level. Post-translational modification of RUNX2 protein exists in many forms. During atherosclerotic calcification, AMPKα1 can promote the pairing of RUNX2 with SUMOy and reduce its stability.[32] PTEN/AKT regulates ubiquitination of RUNX2 by phosphorylating FOXO1/3 in VSMCs.[33] In addition, enhanced acetylation of RUNX2 particles can improve its stability and transcriptional activity.[34,35] Our study found that the degree of RIPK1 activation has an effect on the expression level of RUNX2 protein, and this effect is achieved through TAK1-AMPK pathway affecting SMURF1 binding to RUNX2, thereby changing the ubiquitination level of RUNX2 protein.

In this study, we found a significant correlation between the phosphorylation of the NEDD4 protein and the activation of RIPK1. This discovery is consistent with previous literature that reports the phosphorylation of NEDD4 enhancing its ubiquitination capacity. While our research provides preliminary evidence for this correlation, further experiments are required to ascertain whether the activation of RIPK1 directly enhances the ubiquitination activity of NEDD4. We propose a hypothesis that RIPK1 may indirectly affect the ubiquitination capacity of NEDD4 by influencing its phosphorylation status. We encourage future researchers to experimentally validate this hypothesis and further explore the potential interaction mechanisms between NEDD4 and RIPK1. These studies will contribute to a more comprehensive understanding of the roles of these two proteins in cellular signaling and regulation.

Overall, these results provide insights into the molecular mechanisms underlying VC and may have implications for the development of therapeutic strategies for this condition. The study highlights the potential of targeting RIPK1 for the prevention and treatment of VC.

Limitations of the study

We found a significant correlation between the phosphorylation of the NEDD4 protein and the activation of RIPK1. However, the specific mechanism is still unclear, which is the drawback of this study. Moreover, we did not study the effectiveness of RIPK1 inhibitors in the 5/6

nephropathy model, which is another drawback of our study. In addition, we will further investigate the effect of RIPK1-kinase dead knockin mutant mice, such as RIPK1-D138N or RIPK1-K45M mice, on calcification in follow-up studies.

STAR★METHODS

Detailed methods are provided in the online version of this paper and include the following:

- KEY RESOURCES TABLE
- RESOURCE AVAILABILITY
  - Lead contact
  - Materials availability
  - Data and code availability
- EXPERIMENTAL MODEL AND STUDY PARTICIPANT DETAILS
  - Human samples
  - Ethical approval
  - Informed consent
  - Humane animal care
  - Animal experiments
- METHOD DETAILS
  - Cell culture
  - Immunofluorescence staining and immunohistochemistry
  - Alizarin red staining
  - Quantitative real-time PCR
  - Transfection and transduction of VSMCs
  - Immunoprecipitation and western blot analysis
  - Calcium quantification
  - von Kossa assay
  - Study approval
- QUANTIFICATION AND STATISTICAL ANALYSIS

SUPPLEMENTAL INFORMATION

Supplemental information can be found online at https://doi.org/10.1016/j.isci.2023.108766.

ACKNOWLEDGMENTS

This work was supported by the National Natural Science Foundation of China (82330021, 82270771, and 81870506) and National Key Research and Development Program (2020YFC2004405). Central Military Commission Key Project of Basic Research for Application (BWJ21J003). Key Project of Sustainable Development Science and Technology of Shenzhen Science and Technology Innovation Committee (KCXFZ20211020163801002). Shenzhen Medical Research Fund (B2302020), and Shenzhen Key Medical Discipline Construction Fund (SZXK002), Futian District Public Health Scientific Research Project of Shenzhen (FTWS2022001). Chinese Association of Integrative Medicine-Shanghai Hutchison Pharmaceuticals Fund (HMPE202202).

AUTHOR CONTRIBUTIONS

H.H. conceived the project. Yue Li, W.J., and Y.Q. performed and analyzed *in vivo* experiments. Yue Li, W.J., and Y.Q. performed the *in vitro* experiments and analyzed the data. L.Y., M.M., and Yaxin Lian performed and analyzed the biochemical and biophysical experiments. Yue Li was responsible for human clinical and molecular genetic studies. Yue Li wrote the paper with input from all authors. The images were photographed by Yue Li. The order of co-first authors was determined by their efforts and contributions to the manuscript.

DECLARATION OF INTERESTS

The authors declare no competing interests.

Received: June 29, 2023
Revised: September 5, 2023
Accepted: December 18, 2023
Published: December 20, 2023

REFERENCES

1. Verma, A., Vaidya, A., Subudhi, S., and Waikar, S.S. (2022). Aldosterone in chronic kidney disease and renal outcomes. Eur. Heart J. *43*, 3781–3791.
2. Matsushita, K., Ballew, S.H., Wang, A.Y.M., Kalyesubula, R., Schaeffner, E., and Agarwal, R. (2022). Epidemiology and risk of cardiovascular disease in populations with chronic kidney disease. Nat. Rev. Nephrol. *18*, 696–707.
3. Wang, X., Xu, P., Jiao, Y., Luan, S., Gao, Y., Zhao, C., and Fu, P. (2022). Preliminary evaluation of a small interfering RNA molecular probe targeting murine double minute 2 in breast cancer. Nucl. Med. Commun. *43*, 869–876.
4. Aguilar, A. (2016). Chronic kidney disease: Gli1(+) adventitial cells have a critical role in vascular calcification in CKD. Nat. Rev. Nephrol. *12*, 649.
5. Viegas, C.S.B., Santos, L., Macedo, A.L., Matos, A.A., Silva, A.P., Neves, P.L., Staes, A., Gevaert, K., Morais, R., Vermeer, C., et al. (2018). Chronic Kidney Disease Circulating Calciprotein Particles and Extracellular Vesicles Promote Vascular Calcification: A Role for GRP (Gla-Rich Protein). Arterioscler. Thromb. Vasc. Biol. *38*, 575–587.
6. Ouyang, L., Su, X., Li, W., Tang, L., Zhang, M., Zhu, Y., Xie, C., Zhang, P., Chen, J., and Huang, H. (2021). ALKBH1-demethylated DNA N6-methyladenine modification triggers vascular calcification via osteogenic reprogramming in chronic kidney disease. J. Clin. Invest. *131*, e146985.
7. Chao, C.T., Yeh, H.Y., Tsai, Y.T., Chiang, C.K., and Chen, H.W. (2021). A combined microRNA and target protein-based panel for predicting the probability and severity of uraemic vascular calcification: a translational study. Cardiovasc. Res. *117*, 1958–1973.
8. Chen, Y., Zhao, X., and Wu, H. (2020). Arterial Stiffness: A Focus on Vascular Calcification and Its Link to Bone Mineralization. Arterioscler. Thromb. Vasc. Biol. *40*, 1078–1093.
9. Atta, M.G. (2022). A molecular target of vascular calcification in chronic kidney disease. J. Clin. Invest. *132*, e156257.
10. Li, W., Feng, W., Su, X., Luo, D., Li, Z., Zhou, Y., Zhu, Y., Zhang, M., Chen, J., Liu, B., and Huang, H. (2022). SIRT6 protects vascular smooth muscle cells from osteogenic transdifferentiation via Runx2 in chronic kidney disease. J. Clin. Invest. *132*, e150051.
11. Tomaniak, M., Katagiri, Y., Modolo, R., de Silva, R., Khamis, R.Y., Bourantas, C.V., Torii, R., Wentzel, J.J., Gijsen, F.J.H., van Soest, G., et al. (2020). Vulnerable plaques and patients: state-of-the-art. Eur. Heart J. *41*, 2997–3004.
12. Xu, D., Zhao, H., Jin, M., Zhu, H., Shan, B., Geng, J., Dziedzic, S.A., Amin, P., Mifflin, L., Naito, M.G., et al. (2020). Modulating TRADD to restore cellular homeostasis and inhibit apoptosis. Nature *587*, 133–138.
13. Mifflin, L., Ofengeim, D., and Yuan, J. (2020). Receptor-interacting protein kinase 1 (RIPK1) as a therapeutic target. Nat. Rev. Drug Discov. *19*, 553–571.
14. Newton, K., Dixit, V.M., and Kayagaki, N. (2021). Dying cells fan the flames of inflammation. Science *374*, 1076–1080.
15. Karunakaran, D., Nguyen, M.A., Geoffrion, M., Vreeken, D., Lister, Z., Cheng, H.S., Otte, N., Essebier, P., Wyatt, H., Kandiah, J.W., et al. (2021). RIPK1 Expression Associates With Inflammation in Early Atherosclerosis in Humans and Can Be Therapeutically Silenced to Reduce NF-kappaB Activation and Atherogenesis in Mice. Circulation *143*, 163–177.
16. Ofengeim, D., and Yuan, J. (2013). Regulation of RIP1 kinase signalling at the crossroads of inflammation and cell death. Nat. Rev. Mol. Cell Biol. *14*, 727–736.
17. Li, W., Shan, B., Zou, C., Wang, H., Zhang, M.M., Zhu, H., Naito, M.G., Xu, D., Manuel, V.J., Mifflin, L., et al. (2022). Nuclear RIPK1 promotes chromatin remodeling to mediate inflammatory response. Cell Res. *32*, 621–637.
18. Li, S., Qu, L., Wang, X., and Kong, L. (2022). Novel insights into RIPK1 as a promising target for future Alzheimer's disease treatment. Pharmacol. Ther. *231*, 107979.
19. Steitz, S.A., Speer, M.Y., Curinga, G., Yang, H.Y., Haynes, P., Aebersold, R., Schinke, T., Karsenty, G., and Giachelli, C.M. (2001). Smooth muscle cell phenotypic transition associated with calcification: upregulation of Cbfa1 and downregulation of smooth muscle lineage markers. Circ. Res. *89*, 1147–1154.
20. Speer, M.Y., Yang, H.Y., Brabb, T., Leaf, E., Look, A., Lin, W.L., Frutkin, A., Dichek, D., and Giachelli, C.M. (2009). Smooth muscle cells give rise to osteochondrogenic precursors and chondrocytes in calcifying arteries. Circ. Res. *104*, 733–741.
21. Zhang, X.J., Liu, X., Hu, M., Zhao, G.J., Sun, D., Cheng, X., Xiang, H., Huang, Y.P., Tian, R.F., Shen, L.J., et al. (2021). Pharmacological inhibition of arachidonate 12-lipoxygenase ameliorates myocardial ischemia-reperfusion injury in multiple species. Cell Metab. *33*, 2059–2075.e10.
22. Wei, J., Shimazu, J., Makinistoglu, M.P., Maurizi, A., Kajimura, D., Zong, H., Takarada, T., Lezaki, T., Pessin, J.E., Hinoi, E., and Karsenty, G. (2015). Glucose Uptake and Runx2 Synergize to Orchestrate Osteoblast Differentiation and Bone Formation. Cell *161*, 1576–1591.
23. Deng, L., Huang, L., Sun, Y., Heath, J.M., Wu, H., and Chen, Y. (2015). Inhibition of FOXO1/3 promotes vascular calcification. Arterioscler. Thromb. Vasc. Biol. *35*, 175–183.
24. Bae, H.S., Yoon, W.J., Cho, Y.D., Islam, R., Shin, H.R., Kim, B.S., Lim, J.M., Seo, M.S., Cho, S.A., Choi, K.Y., et al. (2017). An HDAC Inhibitor, Entinostat/MS-275, Partially Prevents Delayed Cranial Suture Closure in Heterozygous Runx2 Null Mice. J. Bone Miner. Res. *32*, 951–961.
25. Neumann, D. (2018). Is TAK1 a Direct Upstream Kinase of AMPK? Int. J. Mol. Sci. *19*, 2412.
26. Persaud, A., Alberts, P., Mari, S., Tong, J., Murchie, R., Maspero, E., Safi, F., Moran, M.F., Polo, S., and Rotin, D. (2014). Tyrosine phosphorylation of NEDD4 activates its ubiquitin ligase activity. Sci. Signal. *7*, ra95.
27. Karunakaran, D., Nguyen, M.A., Geoffrion, M., Vreeken, D., Lister, Z., Cheng, H.S., Otte, N., Essebier, P., Wyatt, H., Kandiah, J.W., et al. (2021). RIPK1 Expression Associates With Inflammation in Early Atherosclerosis in Humans and Can Be Therapeutically Silenced to Reduce NF-κB Activation and Atherogenesis in Mice. Circulation *143*, 163–177.
28. Xu, D., Jin, T., Zhu, H., Chen, H., Ofengeim, D., Zou, C., Mifflin, L., Pan, L., Amin, P., Li, W., et al. (2018). TBK1 Suppresses RIPK1-Driven Apoptosis and Inflammation during Development and in Aging. Cell *174*, 1477–1491.e19.
29. Naik, V., Leaf, E.M., Hu, J.H., Yang, H.Y., Nguyen, N.B., Giachelli, C.M., and Speer, M.Y. (2012). Sources of cells that contribute to atherosclerotic intimal calcification: an in vivo genetic fate mapping study. Cardiovasc. Res. *94*, 545–554.
30. Li, W., Feng, W., Su, X., Luo, D., Li, Z., Zhou, Y., Zhu, Y., Zhang, M., Chen, J., Liu, B., and Huang, H. (2022). SIRT6 protects vascular smooth muscle cells from osteogenic transdifferentiation via Runx2 in chronic kidney disease. J. Clin. Invest. *132*, e150051.
31. Ouyang, L., Yu, C., Xie, Z., Su, X., Xu, Z., Song, P., Li, J., Huang, H., Ding, Y., and Zou, M.H. (2022). Indoleamine 2,3-Dioxygenase 1 Deletion-Mediated Kynurenine Insufficiency in Vascular Smooth Muscle Cells Exacerbates Arterial Calcification. Circulation *145*, 1784–1798.
32. Cai, J., Liu, Z., Huang, X., Shu, S., Hu, X., Zheng, M., Tang, C., Liu, Y., Chen, G., Sun, L., et al. (2020). The deacetylase sirtuin 6 protects against kidney fibrosis by epigenetically blocking β-catenin target gene expression. Kidney Int. *97*, 106–118.
33. Kim, B., Kim, H., Jung, S., Moon, A., Noh, D.Y., Lee, Z.H., Kim, H.J., and Kim, H.H. (2020). A CTGF-RUNX2-RANKL Axis in Breast and Prostate Cancer Cells Promotes Tumor Progression in Bone. Journal of bone *35*, 155–166.
34. Kim, H.J., Kim, W.J., Ryoo, H.M., et al. (2020). Post-Translational Regulations of Transcriptional Activity of RUNX2. Mol. Cells *43*, 160–167.
35. Park, O.J., Kim, H.J., Woo, K.M., Baek, J.H., and Ryoo, H.M. (2010). FGF2-activated ERK mitogen-activated protein kinase enhances Runx2 acetylation and stabilization. J. Biol. Chem. *285*, 3568–3574.

STAR★METHODS

KEY RESOURCES TABLE

REAGENT or RESOURCE	SOURCE	IDENTIFIER
Antibodies		
Rabbit anti-Runx2	Proteintech	Cat:#20700-1-AP
Mouse anti-α-SMA	Abcam	Cat:#ab5694
Rabbit anti-SM22α	Abcam	Cat:#ab14106
Rabbit anti-OPN	ThermoFisher	Cat:#PA527463
Rabbit anti-Smoothelin	Abcam	Cat:#74379
Rabbit anti-RIPK1	Proteintech	Cat:#17519-1-AP
Rabbit anti-p-S166-RIPK1	CST	Cat:#65746
Rabbit anti-p-S166-RIPK1	Proteintech	Cat:AF2398
Rabbit anti-TAK1	CST	Cat:#5206
Rabbit anti-Lkb1	Affinity	Cat:#BF0281
Rabbit anti-Pp2a	Affinity	Cat:#AF4753
Rabbit anti-NEDD4	Proteintech	Cat:#21698-1-AP
Rabbit anti-AMPK	CST	Cat:#2532S
Rabbit anti-*p*-AMPK(Thr172)	CST	Cat:#2535
Rabbit anti-SMURF1	Proteintech	Cat:#55175-1-AP
Rabbit anti-Ub	Proteintech	Cat:A19686
Rabbit anti-GAPDH	Proteintech	Cat:# 60004-1-Ig
Rabbit anti-β-Actin	Proteintech	Cat:#66009-1-Ig
Goat Anti-Rabbit IgG(H + L) Secondary Antibidy	Proteintech	Cat:#B900210
Goat Anti-Mouse IgG(H + L) Secondary Antibidy	Proteintech	Cat:#B900120
Peroxidase-AffiniPure Goat Anti-Rabbit IgG(H + L)	Jackson	Cat:#111-035-003
Biological samples		
Human blood vessel sample	The Eighth Affiliated Hospital of Sun Yat-sen University	N/A
Chemicals, peptides, and recombinant proteins		
Lipofectamine 2000	Thermo Fisher Scientific	Cat:#11668019
Lipofectamine RNAiMAX	Cat:#11668019	Cat:#13778150
DNase	Takara	Cat:#2270A
RNasin	Promega	Cat:#N2115
Recombinant RNase inhibitor	Takara	Cat:#2313A
RNase A	ThermoFishe	Cat:#EN0531
Prime Script RT reagent kit	Takara	RR037A
Critical commercial assays		
BCA Protein Assay Kit	Beyotime	P0012S
Prime Script RT reagent kit	Takara	RR037A
Fluorescent Reagent Kit v2 Assay	Advanced Cell Diagnostics	Cat. No. 323110
Necrostatin-1	Invivochem	V0037
Necrostatin-1S	Selleck	852391-15-2
MG-132	CST	Cat:#2194

(*Continued on next page*)

Continued

REAGENT or RESOURCE	SOURCE	IDENTIFIER
3-Methyladenine	Selleck	Cat:#5142-23-4
Cycloheximide	CST	Cat:#2112
Experimental models: Cell lines		
HAoSMCs	ATCC	Pcs-100-012
Oligonucleotides		
TAK1 siRNA	RIBOBIO	N/A
NEDD4 siRNA	RIBOBIO	N/A
AMPK siRNA	RIBOBIO	N/A
Pp2a siRNA	RIBOBIO	N/A
Lkb1 siRNA	RIBOBIO	N/A
Primer for RT-PCR:RUNX2 Forward: 5′ - TGGTTACTGTCATGGCGGGTA-3′	This paper	N/A
Primer for RT-PCR:RUNX2 Reverse: 5′ -TCTCAGATCGTTGAACCTTGCTA-3′	This paper	N/A
Primer for RT-PCR:TAK1 Forward: 5′ - CCGGTGAGATGATCGAAGCC-3′	This paper	N/A
Primer for RT-PCR:TAK1 Reverse: 5′ -GCCGAAGCTCTACAATAAACGC-3′	This paper	N/A
Primer for RT-PCR:GAPDH Forward: 5′ - GGAGCGAGATCCCTCCAAAAT-3′	This paper	N/A
Primer for RT-PCR:GAPDH Forward: 5′ - GGCTGTTGTCATACTTCTCATGG-3′	This paper	N/A
Software and algorithms		
ImageJ	National Institutes of Health	https://imagej.nih.gov/ij/
GraphPad Prism 9.0	GraphPad Prism Software	https://www.graphpad.com/
ImageLab	Bio-Rad Laboratories	https://chameleonimagelab.com/

RESOURCE AVAILABILITY

Lead contact

Further information and requests for resources should be directed to and will be fulfilled by the lead contact, Hui Huang (huanghui765@126.com).

Materials availability

Cell lines generated in this study will be available upon request from the lead contact.

Data and code availability

- All data reported in this paper will be shared by the lead contact upon request (huanghui765@126.com).
- This paper does not report original code.
- Any additional information required to reanalyze the data reported in this paper is available from the lead contact upon request.

EXPERIMENTAL MODEL AND STUDY PARTICIPANT DETAILS

Human samples

The arteries of patients were collected from The Eighth Affiliated Hospital of Sun Yat-sen University from November 2017 to January 2020. (Ethics NO:SYSU-IACUC-2020-0043S2). Patient specific information is provided in the Table S1.

Human artery samples were collected in The Eighth Affiliated Hospital of Sun Yat-sen University, and the artery samples was removed from patients who underwent an arterial venous fistula operation as previously described.

This study included a total of 22 individuals. Exclusion criteria were as follows: (1) patients who did not undergo chest CT examination; (2) individuals with a history of autoimmune disorders; (3) those with a history of long-term use of immunosuppressive agents; (4) incomplete

data. Ultimately, 15 patients were included, categorized into the control group (Ctrl) and the calcification group (VC) based on Agatston scores. VC patients were defined as Agatston scores >0 in this study.

Assessment of thoracic aorta calcification score. Patients underwent a chest multi-detector computed tomography (MDCT) scan with standard electrocardiographically (ECG) gated protocol to evaluate thoracic aorta calcification. Agatston scores of images were blind-quantified by 3 independent investigators with Siemens Syngo CT Workplace software according to standard criteria. The thoracic aorta refers to the section between the ascending and descending aorta. To measure calcification scores, the CT images were reconstructed with 1 mm–thick slices. The presence of calcification was defined as Agatston score in the present study.

Ethical approval

All the related procedures for human samples were performed with the Declaration of Helsinki and approved by Ethics Committee of Tungwah Hospital of Sun Yat-sen University and The Eighth Affiliated Hospital Sun Yat-sen University (2017DHLL017).

Informed consent

All participants signed informed consent before entering this study. Data obtained from research conducted in human subjects are approved by the institutional review board or Ethics board and that informed consent was obtained as required by the study authorizing entity.

Humane animal care

All animals received humane care in compliance with the 'Principles of Laboratory Animal Care' formulated by the National Society for Medical Research and the 'Guide for the Care and Use of Laboratory Animals' prepared by the Institute of Laboratory Animal Resources and published by the National Institutes of Health.

Animal experiments

AP model

Male mice were used in this study to avoid the potential interference of changing levels of hormones on VC. WT C57BL/6J mice at 8 weeks and weighing 20 to 25 g were purchased from the Laboratory Animal Center of Sun Yat-sen University. All mice were raised in a temperature-controlled room on a 12-h light/dark cycle with available access to food and water. WT mice were randomly assigned to experimental groups with at least 15 animals in each group: the control group was fed with standard normal diet (ND) and the CKD model group was fed with special chow containing 0.2% adenine and high (1.2%) levels of phosphorus (AP). The diets of the mice were synthesized and provided by Guangdong Animal Experiment Center. Nec-1 was dissolved in 0.5% DMSO at a concentration of 5 mg/mL and was injected intraperitoneally at a dose of 1.8 mg/kg body weight every two days for 12 weeks (AP+NEC-1). The control group was injected intraperitoneally with normal saline solution alone; the CKD model group was injected intraperitoneally with DMSO (AP + DMSO); the NEC-1 pretreatment group was injected intraperitoneally with NEC-1. After 12 weeks of AP diet, the animals were analyzed to confirm the vascular calcification of aorta, Then the mice were sacrificed and aortas were collected. The detailed protocols were shown in our previous study. The aorta was harvested from each animal and was kept at −80°C for further use. Blood samples were collected from the eyes of the mice, and the supernatant was centrifuged and kept at −80°C for further use.

VD model

Male mice were used in this study to avoid the potential interference of changing levels of hormones on VC. WT C57BL/6J mice at 8 weeks and weighing 20 to 25 g were purchased from the Laboratory Animal Center of Sun Yat-sen University. All mice were raised in a temperature-controlled room on a 12-h light/dark cycle with available access to food and water. WT mice were randomly assigned to experimental groups with at least 15 animals in each group: the WT mice were fed with standard normal diet (ND). The diets of the mice were synthesized and provided by Guangdong Animal Experiment Center. CKD model was established by intraperitoneal injection of VD solution (VD and VD + DMSO). Nec-1s was dissolved in 0.5% DMSO at a concentration of 5 mg/mL and was injected intraperitoneally at a dose of 10 mg/kg body weight three days (VD+NEC-1s). Then the animals were sacrificed to confirm the vascular calcification of aorta after seven days, then the aortas and kidney were collected. The detailed protocols were shown in our previous study.

METHOD DETAILS

Cell culture

Primary HAoSMCs were purchased from ATCC and cultured in DMEM containing 10% FBS supplemented with 100 U/mL penicillin, 100 μg/mL streptomycin. To induce calcification, VSMCs at 80% confluence were incubated in DMEM containing 10% FBS, 100 U/mL penicillin, and 100 μg/mL streptomycin, with the addition of sodium phosphate (Pi) (Sigma) and cultured at 37°C in an incubator containing 5% CO2 for 7 days. The final concentration of phosphorus was 3.0 mmol/L. The medium and Pi were refreshed every 2 days. The control VSMCs were treated with DMEM containing 10% FBS, 100 U/mL penicillin, and 100 μg/mL streptomycin, but without Pi, and the medium was also refreshed every 2 days. The treatment VSMCs were treated with DMEM containing 10% FBS, 100 U/mL penicillin, 100 μg/mL streptomycin, and Pi, with the addition of NEC-1(10uM), and the medium was also refreshed every 2 days.

Immunofluorescence staining and immunohistochemistry

The VSMCs were first washed with 1× PBS 3 times, and then fixed with 4% paraformaldehyde solution for 20 min. Next, the paraformaldehyde was removed and cells were washed in PBS 3 times. Cells were permeabilized using 0.1% Triton X-. After another 3 PBS washes, cells were incubated with 5% BSA for 30 min. Following this, the primary antibody for rabbit anti-RIPK1 (Proteintech) or rabbit anti-RUNX2 (Proteintech) was incubated overnight at 4°C. Alexa Fluor 488、594–labeled secondary antibodies (Abcam) were incubated for 1 h at room temperature. DAPI (Solarbio) for staining nuclei was incubated for 5 min at room temperature and then cells were washed in PBS 3 times. Imaging was performed using Olympus IX73fluorescence microscope (Olympus). The antibody details can be found in STAR Methods.

Arteries from patients and mice aortic tissues were formalin-fixed and further embedded with paraffin. For immunostaining, tissue sections were deparaffinized in xylene and rehydrated through a graded alcohol series to distilled water. Antigen retrieval was performed by microwave irradiation in ethylene diamine tetraacetic acid (EDTA). Then tissue sections were incubated with 5% normal goat serum in PBS/0.1% Triton X-100 for 1 h at room temperature to reduce nonspecific background staining. Sections were then incubated overnight at 4°C with primary antibody for mouse anti-α-SMA (Abcam), or rabbit anti-RUNX2 (Proteintech). For IF, binding of primary antibodies was visualized using goat anti-rabbit FITC-labeled antibody incubated for 1 h at room temperature. Nuclei were counterstained with DAPI. Prolong Gold antifade reagent was used to decrease fluorescence quenching of the slides. The primary antibodies are listed in STAR Methods.

Alizarin red staining

At collection time points, medium was removed and cultured VSMCs were washed with 4°C PBS 3 times (3 min each wash), and then cell layers were fixed in 4% paraformaldehyde in PBS for 20 min. Next, the paraformaldehyde was removed and the cells were washed in distilled water 3 times (2 min each wash). The cells were then exposed to Alizarin red staining solution (pH 4.2, 1%) for 30 min at room temperature, then washed again with distilled water. Positively stained VSMCs presented a reddish color to indicate the calcification.

Quantitative real-time PCR

Total RNA was extracted from aortic tissue and VSMCs by using Trizol Reagent (Takara) according to the manufacturer's instructions. For mRNA quantification, a PrimeScriptRT Reagent Kit (Takara) was used for RNA reverse transcription into cDNA. Real-time PCR was performed with SYBR Green (Takara) and data were collected and analyzed using a LightCycler 96 real-time system (Roche Diagnostics). Relative quantification was calculated according to the 2ΔΔCt method, with GAPDH level as a reference. The primer sequences are listed in STAR Methods.

Transfection and transduction of VSMCs

For siRNA transfection, VSMCs were plated at 5 × 10^5 cells in 6-well plates. At 50% confluence, cells transfected with specific siRNA at a final concentration of 10 nmol/L with Lipofectamine RNAiMAX Transfection Reagent (thermo Fisher) according to the manufacturer's instructions. After 4 h of transfection with opti-MEM, the DMEM containing 10% FBS was replaced. The full-length of the target gene cDNA was amplified from a mouse cDNA library using standard PCR techniques and inserted into pcDNA3.1. The siRNA are listed in STAR Methods.

Immunoprecipitation and western blot analysis

VSMCs were lysed with lysis buffer (Beyotime) together with protease and phosphatase inhibitors on ice for 20 min. The lysate was then sonicated on ice at 10% power for 2 min. After centrifugation at 12,000*g* for 25 min at 4°C, the supernatant was precleared by incubation with protein A + G magnetic beads (Millipore) and IgG (CST) for 1 h at 4°C. The samples were then place in a magnetic separator for 1 min. The supernatant was incubated with indicated antibody overnight at 4°C on a rotating platform. Protein A + G magnetic beads were then added to the supernatants and incubated for 2 h at room temperature. The immunocomplexes were washed 3 times with the lysis buffer, boiled at 95°C for 10 min with 2× SDS sample buffer, and analyzed by Western blot. For Western blot analysis, the cells lysates or tissue pieces were prepared by adding the lysis buffer on ice for 20 min, supplemented with protease and phosphatase inhibitors, scraping into a 1.5 mL tube, and centrifuging for 25 min at 12,000 *g* at 4°C. The protein content was measured by enhanced BCA protein assay kit (Beyotime). The proteins were boiled in loading buffer (Beyotime) at 100°C for 10 min. Equal amounts of proteins were separated on SDS-polyacrylamide gels and transferred to PVDF membranes (Millipore). The membranes were incubated with the primary antibodies overnight at 4°C. The membranes were then incubated with secondary anti-rabbit (Proteintech) or anti-mouse (Proteintech) HRP-conjugated antibody (diluted 1:10000) for 1 h at room temperature. Antibody binding was detected with ECL detection reagent (Millipore). The relative quantification of immunoblots was analyzed by grayscale in ImageJ. The antibodies used in this study are listed in STAR Methods.

Calcium quantification

Aortic tissues without adventitia were incubated with 0.6 mol/L HCl overnight at 37°C. The supernatant of these tissues was then collected. The cultured VSMCs were washed softly with PBS for 3 times (2 min each wash) and incubated with 0.6 mol/L HCl overnight at 4°C. The supernatant was collected. Calcium content was determined by using a commercial kit (Biosino Bio-Technology and Science) according to the manufacturer's instructions.

von Kossa assay

To examine aorta calcification, slides were dehydrated and rinsed rapidly in double distilled water. The vascular tissue sections were then incubated with 5% silver nitrate solution and exposed to ultraviolet light for 1 h until color development was complete. Next, the slides were incubated with 5% sodium thiosulfate and washed with double distilled water. The slides were photographed by microscopy (Nikon). Calcified nodules were stained brown to black.

Study approval

All the related procedures for collection of the samples of patients were performed with the approval from the internal review and ethics board of Sun Yat-sen University. All participants signed informed consent before entering this study. Experimental animal protocols were approved by the Institutional Animal Care and Use Committee of Sun Yat-sen University.

QUANTIFICATION AND STATISTICAL ANALYSIS

Statistical analyses were performed with the Graphpad Prism v6.00 for Windows (GraphPad Software Inc.). Student's *t* test was used to compare 2 groups and 1-way ANOVA followed by Dunnett's test was used for more than 2 groups. VC Agatston scores were nonnormalized parameters, and logarithmic transformation of VC Agatston scores was used in correlation analysis (Pearson Correlation Analysis).